# Low energy ion distribution measurements in Madison Symmetric Torus plasmas

J. B. Titus, E. D. Mezonlin, and J. A. Johnson III

Citation: Physics of Plasmas (1994-present) **21**, 062511 (2014); doi: 10.1063/1.4883645
View online: http://dx.doi.org/10.1063/1.4883645
View Table of Contents: http://scitation.aip.org/content/aip/journal/pop/21/6?ver=pdfcov
Published by the AIP Publishing



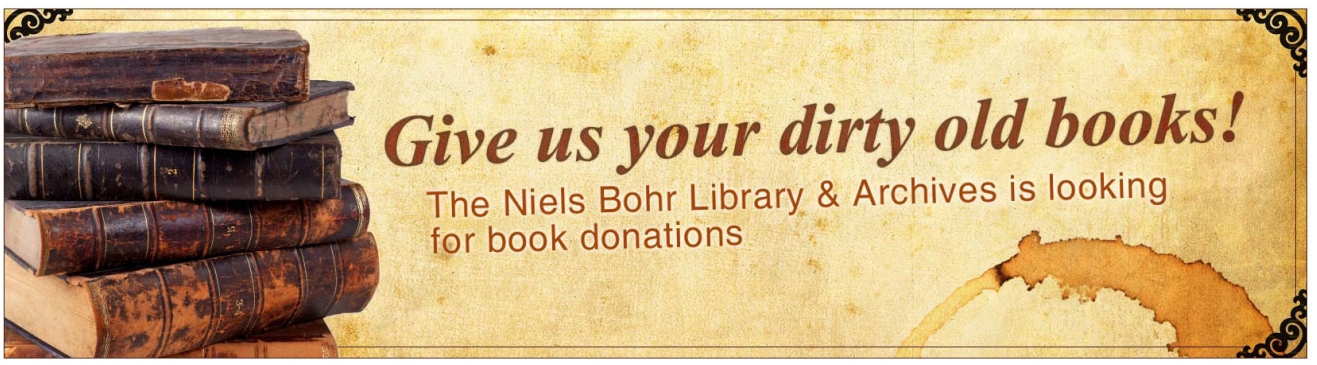

# Low energy ion distribution measurements in Madison Symmetric Torus plasmas

J. B. Titus,[1,a)] E. D. Mezonlin,[1] and J. A. Johnson III[2]
[1]*Florida A&M University, Tallahassee, Florida 32310, USA*
[2]*Pyramid Plasmas LLC, Lawrenceville, Georgia 30043, USA*

(Received 8 May 2014; accepted 4 June 2014; published online 17 June 2014)

Charge-exchange neutrals contain information about the contents of a plasma and can be detected as they escape confinement. The Florida A&M University compact neutral particle analyzer (CNPA), used to measure the contents of neutral particle flux, has been reconfigured, calibrated, and installed on the Madison Symmetric Torus (MST) for high temperature deuterium plasmas. The energy range of the CNPA has been extended to cover 0.34–5.2 keV through an upgrade of the 25 detection channels. The CNPA has been used on all types of MST plasmas at a rate of 20 kHz throughout the entire discharge (~70 ms). Plasma parameter scans show that the ion distribution is most dependent on the plasma current. Magnetic reconnection events throughout these scans produce stronger poloidal electric fields, stronger global magnetic modes, and larger changes in magnetic energy all of which heavily influence the non-Maxwellian part of the ion distribution (the fast ion tail). © *2014 AIP Publishing LLC*. [http://dx.doi.org/10.1063/1.4883645]

## I. INTRODUCTION

High energy resolution ion distribution measurements of bulk and fast ions in the low energy range are measured in MST plasmas. Fast neutrals are born in a plasma due to charge-exchange between the plasma ions and the residual neutral particles. These charge-exchange neutrals, still containing information about plasma ions, can escape the magnetic confinement.[1] To infer information about the ions and their distribution, neutral particle analyzers (NPA) convert collimated beams of neutrals into ions using a stripping cell. These secondary ions are directed according to their energy and mass into detectors with electric and magnetic fields. Ion distribution measurements are useful because they can diagnose the bulk ion temperature, the power lost due to charge-exchange and the effects of ion energization, all of which are important for understanding particle transport and confinement in magnetically confined plasma.

There are many types of neutral particle anaylzers designed for different plasma parameters and regimes. A review of charge-exchange neutral particle analyzers on magnetic confinement fusion devices can be found in Ref. 2. Compact neutral particle analyzers (CNPA) were first developed at the Ioffe Physical-Technical Institute of the Russian Academy of Sciences[3] and have been in use at many different facilities for their small size and high energy resolution capabilities.[4–7] The Florida A&M University CNPA was first used to measure ion distributions in hydrogen, spheromak plasmas[8] on the Sustained Spheromak Physics Experiment, with ion temperatures in the range of 100–250 eV.[4] The diagnostic was upgraded and calibrated for MST's deuterium plasmas, which can have ion temperatures greater than 1 keV.[9]

The ion distribution was first measured in MST plasmas by a five channel charge-exchange analyzer (0.25–3.5 keV) (Ref. 10) and a non-Maxwellian tail (of fast ions) was measured prior to the peak of global magnetic reconnection events (sawtooth crashes). After the CNPA was installed on MST, the fast ion tail was measured with higher energy resolution.[11] An advanced neutral particle analyzer[12,13] (10 channels each of helium and deuterium, 10–45 keV, 2–4 keV energy resolution) has since made measurements of the fast ion distribution in MST discharges featuring 1 MW neutral beam injection.[14] Magnetic reconnection was shown to drive ion energization of these injected ions. Although the fast ion tail had been measured, the influence of different plasma parameters had on it had not yet been studied in detail.

Results of interest include the dependence of the distribution on various plasma parameters, the power loss due to charge-exchange, and energization of the fast ion tail (due to changes in magnetic energy, global magnetic modes, and poloidal electric fields).

## II. APPARATUS AND EXPERIMENT

MST is a toroidal confinement device that operates primarily as a reversed-field pinch. Plasmas are created in an aluminum torus with a major radius of 1.5 m ($R_0$), a minor radius of 0.52 m (a), and a thickness of 0.05 m.[10,15,17] The torus acts as the vacuum vessel, the conducting shell and the toroidal field winding (single turn). Discharges can have plasma currents from 200 to 600 kA and electron densities on the order of $\sim 10^{13}$ cm$^{-3}$.[15] MST discharges are typically deuterium plasmas lasting ~70 ms with ion energies up to 40 keV (using neutral beam injection, NBI).[12]

To make measurements on MST, the CNPA needed to be upgraded and calibrated for deuterium with ion temperatures between 0.1 and 2 keV. This consisted of increasing the instruments detection energies, adapting the diagnostic to detect deuterium and increasing the time gate of the measurements. To increase the energy range and detect deuterium, the magnetic gap and detector array had to be modified. The two-dimensional non-uniform magnet gap is

a)Electronic mail: jtitus@cepast.famu.edu

 

spatially designed to provide focusing of the ions into the detectors. Thicker permanent magnets were installed, increasing the magnetic field at the magnetic gap by a factor of 3.3. The distance between the array and the central plane of the magnetic gap was increased by a factor of 2. The detectors were then adjusted to provide an energy range of 0.34–5.2 keV. To increase the duration of the measurement, the inlet and outlet slits of the gas stripping cell were decreased from 2 to 1 mm to increase the confinement time of the gas in the cell. The duration of the measurement was increased to ~70 ms with a maximum data rate of 20 kHz. With the large number of channels and broad energy range, measurements of the bulk ion distribution with a fast ion tail and an approximate effective ion temperature for different parts of the plasma along the line-of-sight can be made. The CNPA has a radial view of MST plasmas and is located at 330° toroidal and 15° poloidal, shown in Fig. 1.

### A. Initial measurements

During the initial measurements of the CNPA at MST, it was found that a strong signal was detected without gas being puffed into the stripping cell. Stray ions were being detected by the CNPA because the stochastic magnetic fields in typical plasma discharges drive particle transport toward the edge,[18] where some escape confinement. Two 4 inch "U"-shaped magnets were installed above and below the vacuum line between the CNPA and MST to deflect incoming ions from entering the CNPA. The signal before any alterations to CNPA's flight tube is shown in black in Fig. 2. After the magnets were installed, the magnetic field lines produced by both magnets altered the ion trajectories so that the signal from them was significantly reduced, shown in red, in Fig. 2. The blue trace in Fig. 2, the signal with the magnets in place and gas being puffed into the stripping cell, is, then, the most accurate signal without noise from stray ions.

After the initial measurements were done, error from random electronic noise and UV light was calculated. The electronic noise was calculated from the r.m.s. of the signal, while the CNPA was closed off to MST during a shot. The UV noise was calculated from the r.m.s. of the signal, while the CNPA was opened to MST during a shot without gas puffing. The total signal due to these sources is two orders of magnitude less than the signal during plasma shots, while puffing gas into the stripping cell.

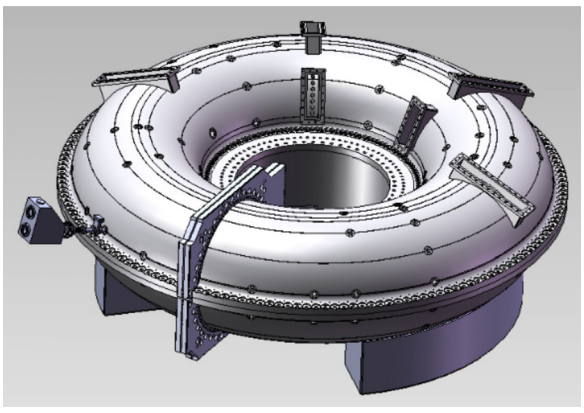

FIG. 1. The CNPA on a radial view port of MST (330° toroidal and 15° poloidal).

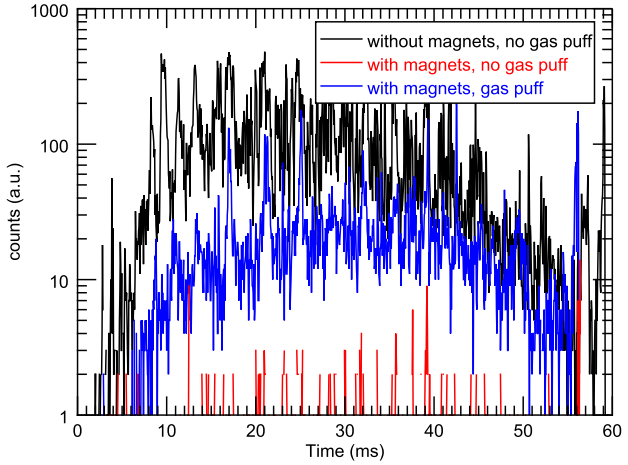


FIG. 2. CNPA ch.2 (0.39 keV) signal versus time with: no magnets or gas puffing (black), magnets installed with no gas puffing (red), and magnets installed with gas puffing (blue).

The experimental neutral flux, $\Gamma(E)$, is related to the ion distribution, $f_i$, in the time interval $\Delta t$ by[1]

$$\frac{\Gamma(E)}{E\sigma_{cx}} = \int_{-a}^{a}\left[-\int_{z}^{a}\alpha(E,l)dl\right]n_\alpha(x)f_i(v_i,x)dx, \qquad (1)$$

where $E$ is the energy per channel, $\sigma_{cx}$ is the charge-exchange cross section, $n_\alpha(x)$ is the neutral profile, and $\Gamma(E)$ is given by

$$\frac{N(E)}{\Delta E\cdot\alpha(E)\cdot p_{str}\cdot A\Omega\cdot\Delta t}\,[\#/\mathrm{eV}/\mathrm{cm}^2/\mathrm{ster}/\mathrm{s}]. \qquad (2)$$

Here, $N(E)$ is the counts per energy channel, $\Delta E$ is the width of the energy channel, $\alpha(E)$ is the efficiency of each channel, $p_{str}$ is the stripping pressure, and $A\Omega$ is the etendue of the detector [ster cm$^2$]. If $d_1$, $d_2$ are the diameters of the slits of the stripping cell and $R_{12}$ is the distance between the slits, then, $\Omega = 0.62\frac{d_1^2\cdot d_2^2}{R_{12}^2}$.[16] The energy resolution (between 7.0% and 15.9%) and detection efficiency was measured during the calibration of the CNPA at the Ioffe Physical-Technical Institute.[16]

A typical plasma discharge with plasma current and the average toroidal magnetic field, $\langle B_T\rangle$, is shown in Fig. 3, along with two CNPA parameters: stripping cell pressure and the detected counts from the 17th detector (2.75 keV) in the array. The data show sawteeth-like structure in the $\langle B_T\rangle$ and in CNPA signals.[17] These sawteeth events correspond to reconnection events, where magnetic flux is generated and ions are non-collisionally heated.[19] The analysis of all diagnostic measurements is best during the flat top segment (approximately 15 to 35 ms) of the discharge, highlighted in Fig. 3, where any evolution is not correlated to ramping or decay of plasma current. The ion distributions during a plasma discharge are shown in Fig. 4.

## III. DATA ANALYSIS

As shown in Fig. 4, the ion distribution evolves throughout the plasma discharge. The inferred ion distribution is

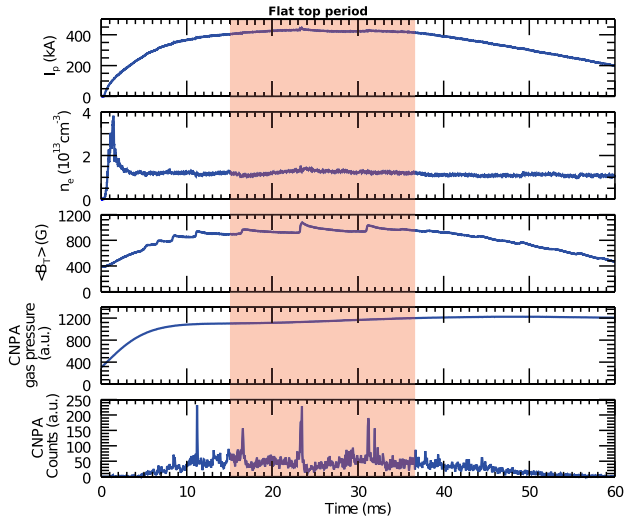


FIG. 3. An example of a 400 kA, F = −0.2, $n_e = 0.5 \times 10^{13}$ cm$^{-3}$ plasma discharge. Plasma parameters: (a) plasma current and (b) average toroidal magnetic field, $\langle B_T \rangle$. CNPA parameters: (c) gas pressure in the stripping cell and (d) neutral flux counts from the 8th detector (0.99 keV). The flat top of the plasma current is highlighted.

affected by charge-exchange and ion energization. The evolution is dictated mainly by the plasma parameters: electron density, plasma current, and $F = \langle B_T \rangle / B_T(a)$, where $B_T(a)$ is the toroidal magnetic field at the wall. Subsections III A–III C present how changes in plasma parameters influence the distribution of ions, power losses due to charge-exchange and ion energization. All ion distributions shown are statistically ensembled about the plasma parameters specified to within 10% of the stated value.

### A. Ion distributions with respect to plasma parameters

Statistically ensembled ion distributions during plasma parameter scans are shown in Fig. 5. During the plasma current scan (Fig. 5(a)), the current was increased in increments of 100 kA (at $n_e \sim 0.7 \times 10^{13}$ cm$^{-3}$). As the plasma current is increased, the fast ion tail increases and the bulk part of the distribution (< 1 keV) remains fairly constant. The lower plasma currents (200, 300 kA) show large error bars in the fast ion tail, near the noise threshold due to lack of counts. The lower bulk distribution in the 500 kA case may be due to a slightly lower electron density than the other ensembles because, as the electron density is increased, (Fig. 5(b)) the ion distribution decreases across the entire energy spectrum. This is because the charge-exchange cross section is linearly dependent on electron density but non-linearly dependent on temperature. In MST, as electron density increases the temperature decreases and there is less charge-exchange. As the toroidal field amplitude at the wall decreases (and F increases toward zero), the ion distribution decreases across the entire energy spectrum (Fig. 5(c)). When the parameter F = 0, the poloidal number $m = 0$ perturbation no longer couples with $m = 1$, $n = 5, 6, 7$ magnetic modes (poloidal and toroidal magnetic numbers, respectively) and global reconnection is suppressed.[19] Since there are no global reconnection events, the overall temperature is relatively lower, charge-exchange is decreased and the distributions decrease.

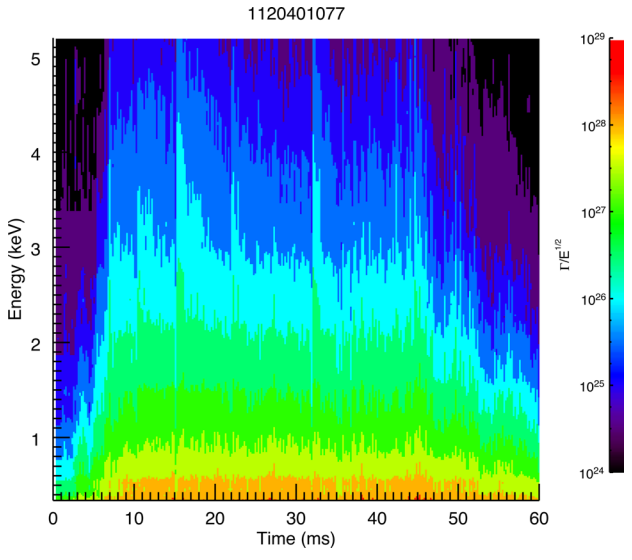


FIG. 4. Contour plot of ion distributions during a 500 kA, F = −0.2, $n_e = 0.8 \times 10^{13}$ cm$^{-3}$ plasma discharge.

### B. Power losses due to charge-exchange

The power lost due to charge-exchange is a function of particle transport and can affect plasma confinement.[21] It was previously measured that the losses were relatively insignificant,[10] but it was not known if the significance changes throughout the discharge. The ratio of power loss from charge exchange to Ohmic heating during a typical 400 kA, F = −0.2 plasma discharge is shown in Fig. 6. Power due to Ohmic heating is given by

$$P_{\text{Ohmic}} = 4\pi^2 R_0 \int_0^a \eta J_{\parallel}^2 dV = V_p I_p + V_t I_t - \Delta U_{mag}, \quad (3)$$

where $\eta$ is the resistivity, $J_{\parallel}$ is the parallel plasma current, $V_{p,t}$ are the poloidal and toroidal voltages, $I_{p,t}$ the poloidal and toroidal plasma current, and $\Delta U_{mag}$ is the change in magnetic energy.[20] The power loss due to charge-exchange is given by

$$P_{\text{loss}} = e\pi A_{\text{MST}} \int_{E_{min}}^{E_{max}} \Gamma(E) E dE. \quad (4)$$

The power loss due to charge-exchange throughout the shot is insignificant, agreeing with previous measurements. The two spikes, seen in the percentage ratio, occur because of dramatic changes in the measured Ohmic heating. This percentage never becomes a large fraction regardless of plasma parameters.

### C. Ion energization

During sawtooth crashes in MST plasmas, global magnetic reconnection redistributes energy and particles throughout the plasma. The associated magnetic modes ($m = 0$; $m = 1$, $n = 5, 6$) are shown, along with plasma parameters in

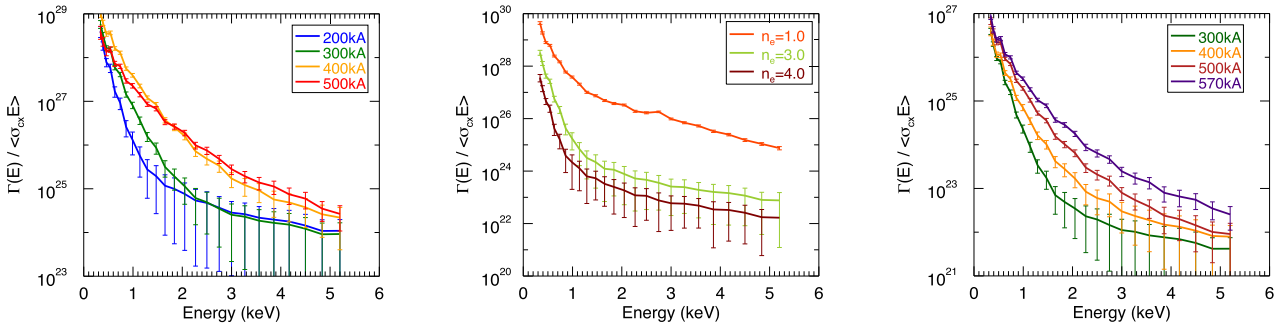


(a) Plasma current scan of ion distributions during a sawtooth crash (F=-0.2).

(b) Electron density scan of ion distributions with F=-0.2.

(c) Plamsa current scan of ion distributions with F=0.

FIG. 5. Examples of ion distributions during plasma parameter scans.

Fig. 7 during a discharge. The peaks in high CNPA energy channels (>1 keV) correspond to $m=0$ activity.

Figure 8 shows three different distribution measurements around an ensembled sawtooth crash. Approximately 1.5 ms before the crash, the plasma is close to equilibrium and there is a non-Maxwellian tail. Right at the crash, the fast ion tail decreases slightly before being energized at ~200 $\mu$s after the crash. This indicates that during the crash, there is a lack of particles available at certain pitch angles to be scattered.

With an increase in plasma current, the poloidal electric field (as approximated by the voltage at the toroidal gap, VTG),[22] change in magnetic energy and strength of the global magnetic mode ($m=0$) during the crash increases. Figure 9 plots these parameters with the change in the percent ratio between the flux of the fast ion population (>1 keV) to the entire distribution, $\Delta(\Gamma_{fi}/\Gamma)\%$. While the strength of the $m=0$ mode increases ~5 times during the plasma current scan, the change in magnetic energy and VTG increases ~10 times. During the 200 kA cases, the percent ratio change is ~0.001%, but at the 500 kA cases, the percent ratio change is ~1.0%, showing that this percent ratio changes 1000 times, while the plasma parameters only change between 5 and 10 times. In contrast, it is also shown in Fig. 9 that a change in electron density by ~20% does not affect the percent ratio. This suggests that the strength of the global magnetic mode and how it affects the change in magnetic energy is very important to ion transport.

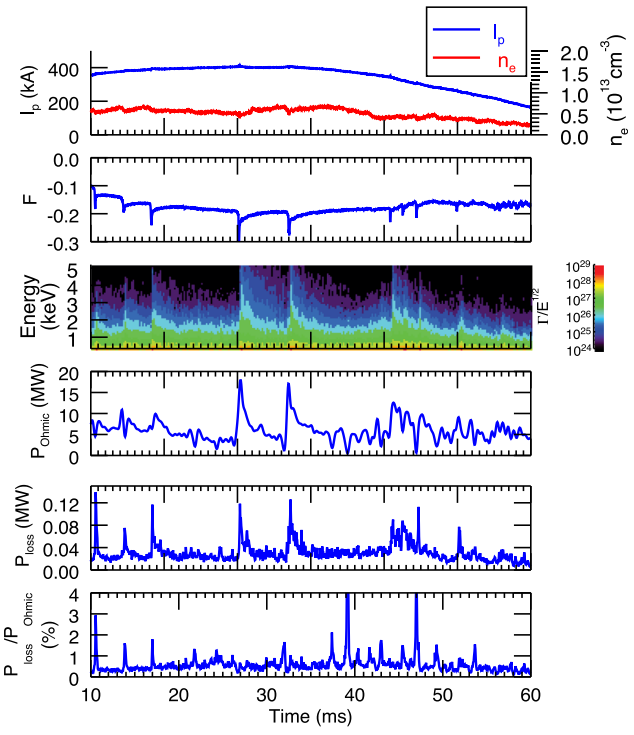


FIG. 6. An example of a 400 kA, F = −0.2, $n_e = 0.5 \times 10^{13}$ cm$^{-3}$ plasma discharge. (a) Plasma current and electron density, (b) F, (c) contour plot of the ion distribution, (d) particle emission, (e) power emission, and (f) $D^0$ average energy vs. time.

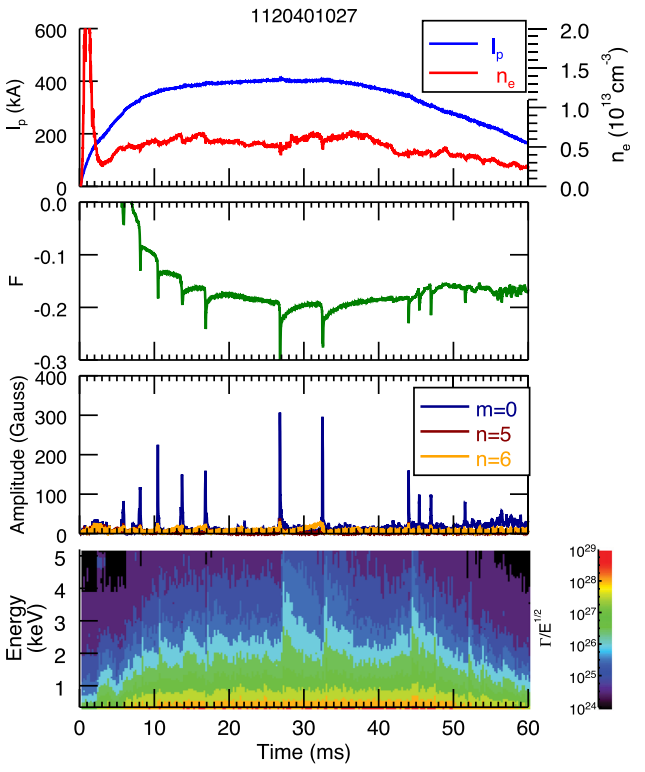


FIG. 7. An example of a 400 kA, F = −0.2, $n_e = 0.5 \times 10^{13}$ cm$^{-3}$ plasma discharge. (a) Plasma current and electron density, (b) F parameter, (c) magnetic mode amplitudes ($m=0$; $m=1$, $n=5$, 6), (d) contour plot of the ion distribution.

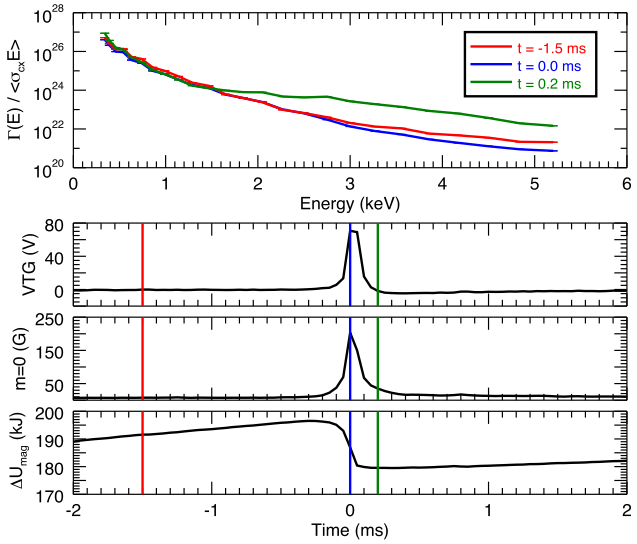


FIG. 8. The evolution of magnetic properties during a sawtooth crash.

## IV. SUMMARY

Measurements of low energy ion distributions have been made on the Madison Symmetric Torus reversed-field pinch. The newly modified analyzer has been used on a wide variety of plasmas and has performed to its full capability in most situations, though at low current, the counts are too low to make any significant conclusion about the fast ion tail. The CNPA provides advantages over the previous charge-exchange analyzers on MST because of it high energy resolution and usefulness during the entire discharge.

Measurements of inferred ion distributions have been made, while scanning the integral plasma parameters: plasma current, electron density, and F (toroidal field at the wall). Increasing the plasma current increases the non-Maxwellian part of the tail. Increasing the electron density and lowering the amplitude of the toroidal magnetic field near the wall decreases the entire distribution. These results all correlate to the ion temperature, i.e., increasing the plasma current increases the temperature of the plasma, just as increasing the electron density and decreasing the field at the wall decreases the temperature of the plasma. The change in distributions does not affect the power lost due to charge-exchange throughout the discharge. It continues to be minimal unless there is a sudden drop in the Ohmic heating measurement.

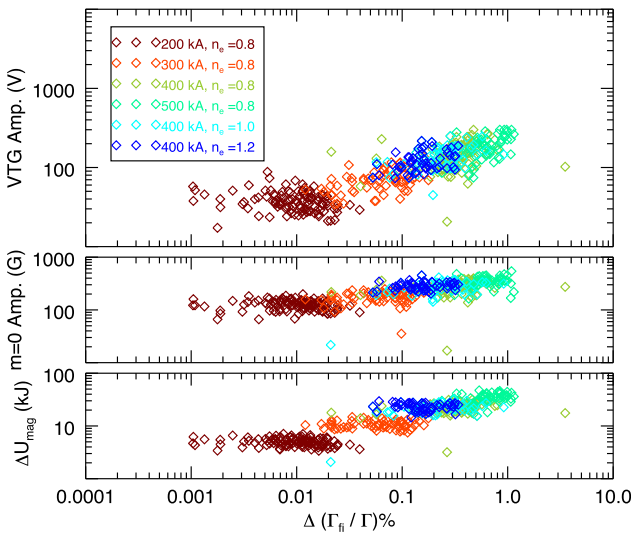


FIG. 9. The change in plasma features: (a) VTG (poloidal electric field), (b) global magnetic mode ($m=0$), and (c) change in magnetic energy, with respect to the percent change in ratio between the fast ion part of the distribution and the whole distribution, for different plasma currents and electron densities around the sawtooth crash.

During sawtooth oscillations in MST discharges, global magnetic reconnection occurs causing ion energization that is detected by the changes in the ion distribution. These $m=0$ magnetic mode bursts correlate to peaks in the fast ion tail. As the plasma current is increased, VTG, the magnetic energy released and the $m=0$ global mode all increase in amplitude, causing the population of fast ions to increase. These measurements suggest that the global magnetic mode plays a part in reducing magnetic energy, and increasing the fast ion population, though the mechanism is still unclear as to how the magnetic energy is converted to kinetic energy.

## ACKNOWLEDGMENTS

We wish to acknowledge the support of the entire MST Team for help with the relocation of the CNPA, specifically A. F. Almagri, J. K. Anderson, Steve Limbach, and Bill Zimmerman during the installation. We would also like to acknowledge the work and support of Ioffe Physical-Technical Institute of the Russian Academy of Sciences, with a special thanks to D. V. Makarin and. F. V. Chernyshev. The authors would finally like to thank the funding support from the U.S. Department of Energy.

[1]I. H. Hutchinson, *Principles of Plasma Diagnostics* (Cambridge University Press, Cambridge, 1987).
[2]S. S. Medley, A. J. H. Donne, R. Kaita, A. I. Kislyakov, M. P. Petrov, and A. L. Roquemore, Rev. Sci. Instrum. **79**, 011101 (2008).
[3]F. V. Chernyshev, V. I. Afanasyev, A. V. Dech, M. Kick, A. I. Kislyakov, S. S. Kozlovskii, A. Kreter, M. I. Mironov, M. P. Petrov, and S. Y. Petrov, Instrum. Exp. Tech. **47**, 214 (2004).
[4]E. D. Mezonlin, S. Roberson, C. Raynor, R. Appartaim, J. A. Johnson III, V. I. Afanasyev, S. S. Kozlovsky, J. M. Moller, D. N. Hill, E. B. Hooper, H. S. McLean, and R. D. Wood, Rev. Sci. Instrum. **78**, 053504 (2007).
[5]W. Schneider, M. R. Turnyanskiy, F. V. Chernyshev, V. I. Afanasyev, M. Kick, and T. Richert, Vacuum **83**, 752 (2008).
[6]R. Balbín, S. Petrov, J. M. Fontdecaba, K. J. McCarthy, V. I. Vargas, J. M. Carmona, J. Guasp, and D. Makarin, in *Proceedings of the 32nd EPS Conference on Plasma Physics, ECA, Vol. 29C* (Tarragona, 2005).
[7]A. N. Karpushov, B. P. Duval, C. Schlatter, V. I. Afanasyev, and F. V. Chaernyshev, Rev. Sci. Instrum. **77**, 033504 (2006).
[8]T. R. Jarboe, Plasma Phys. Controlled Fusion **36**, 945 (1994).
[9]B. E. Chapman, A. F. Almagri, J. K. Anderson, D. L. Brower, K. J. Caspary, D. J. Clayton, D. Craig, D. J. Den Hartog, W. X. Ding, D. A. Ennis, G. Fiksel, S. Gangadhara, S. Kumar, R. M. Magee, R. O'Connell, E. Parke, S. C. Prager, J. A. Reusch, J. S. Sarff, H. D. Stephens, and Y. M. Yang, Plasma Physics Controlled Fusion **52**, 124048 (2010).
[10]E. Scime, M. Cekic, D. J. Den Hatog, S. Hokin, D. J. Holly, and C. Watts, Phys. Fluids B **4**, 4062 (1992).
[11]R. M. Magee, D. J. Den Hartog, S. T. A. Kumar, A. F. Almagri, B. E. Chapman, G. Fiksel, V. V. Mirnov, E. D. Mezonlin, and J. B. Titus, Phys. Rev. Lett. **107**, 065005 (2011).
[12]S. Eilerman, J. K. Anderson, J. A. Reusch, D. Liu, G. Fiksel, S. Polosatkin, and V. Belykh, Rev. Sci. Instrum. **83**, 10D302 (2012).
[13]J. A. Reusch, J. K. Anderson, V. Belykh, S. Eilerman, D. Liu, G. Fiksel, and S. Polosatkin, Rev. Sci. Instrum. **83**, 10D704 (2012).

[14]J. Waksman, J. K. Anderson, M. D. Nornberg, E. Parke, J. A. Reusch, D. Liu, G. Fiksel, V. I. Davydenko, A. A. Ivanov, N. Stupishin, P. P. Deichuli, and H. Sakakita, Phys. Plasmas **19**, 122505 (2012).
[15]M. D. Wyman, B. E. Chapman, J. W. Ahn, A. F. Almagri *et al.*, Nucl. Fusion **49**, 015003 (2009).
[16]Ioffe Physical-Technical Institute of the Russian Academy of Sciences, St. Petersburg, Compact Neutral Particle Analyzer CNPA-05-2: Technical Description and Instruction Manual, 2010.
[17]S. C. Prager, A. F. Almagri, S. Assadi, J. A. Beckstead, R. N. Dexter, D. J. D. Hartog, G. Chartas, S. A. Hokin, T. W. Lovell, T. D. Rempel, J. S. Sarff, W. Shen, C. W. Spragins, and J. C. Sprott, Phys. Fluids B **2**, 1367 (1990).
[18]W. X. Ding, D. L. Brower, D. Craig, B. E. Chapman, D. Ennis, G. Fiksel, S. Gangadhara, D. J. Den Hartog, V. V. Mirnov, S. C. Prager, J. S. Sarff, V. Svidzinski, P. W. Terry, and T. Yates, Phys. Plasmas **15**, 055901 (2008).
[19]S. Hokin, A. Almagri, S. Assadi, J. Beckstead, G. Chartas, N. Crocker, M. Cudzinovic, D. D. Hartog, R. Dexter, D. Holly, S. Prager, T. Rempel, J. Sarff, E. Scime, W. Shen, C. Spragins, C. Sprott, G. Starr, M. Stoneking, and C. Watts, Phys. Fluids B **3**, 2241–2246 (1991).
[20]J. C. Sprott, Phys. Fluids **31**, 2226 (1988).
[21]D. E. Voss and S. A. Cohen, J. Nucl. Mater. **93/94**, 405–412 (1980).
[22]B. E. Chapman, A. F. Almagri, M. Cekic, D. J. D. Hartog, S. C. Prager, and J. S. Sarff, Phys. Plasmas **3**, 709 (1996).